CHEMICAL ABUNDANCES IN 12 RED GIANTS OF THE LARGE MAGELLANIC CLOUD FROM HIGH-RESOLUTION INFRARED SPECTROSCOPY[1]

Verne V. Smith,[2,3] Kenneth H. Hinkle,[4] Katia Cunha,[3,5] Bertrand Plez,[6] David L. Lambert,[7] Catherine A. Pilachowski,[8] Beatriz Barbuy,[9] Jorge Meléndez,[10] Suchitra Balachandran,[11] Michael S. Bessell,[12] Douglas P. Geisler,[13] James E. Hesser,[14] and Claudia Winge[15]

ABSTRACT

High-resolution infrared spectra ($\lambda/\Delta\lambda = 50,000$) have been obtained for 12 red giant members of the Large Magellanic Cloud (LMC) with the Gemini South 8.3 m telescope and Phoenix spectrometer. Two wavelength regions, at 15540 and 23400 Å, were observed. Quantitative chemical abundances of carbon (both ^{12}C and ^{13}C), nitrogen, and oxygen were derived from molecular lines of CO, CN, and OH, while sodium, scandium, titanium, and iron abundances were obtained from neutral atomic lines. The 12 LMC red giants span a metallicity range from $[Fe/H] = -1.1$ to $[Fe/H] = -0.3$. It is found that values for both $[Na/Fe]$ and $[Ti/Fe]$ in the LMC giants fall below their corresponding Galactic values (at these same $[Fe/H]$ abundances) by about ~ 0.1–0.5 dex; this effect is similar to abundance patterns found in the few dwarf spheroidal galaxies with published abundances. The program red giants all show evidence of first dredge-up mixing of material exposed to the CN cycle, that is, low $^{12}C/^{13}C$ ratios and lower ^{12}C with higher ^{14}N abundances. The carbon and nitrogen trends are similar to what is observed in samples of Galactic red giants, although the LMC red giants seem to show smaller $^{12}C/^{13}C$ ratios for a given stellar mass. This relatively small difference in the carbon isotope ratios between LMC and Galactic red giants could be due to increased extra mixing in stars of lower metallicity, as suggested previously in the literature. Comparisons of the oxygen-to-iron ratios in the LMC and the Galaxy indicate that the trend of $[O/Fe]$ versus $[Fe/H]$ in the LMC falls about 0.2 dex below the Galactic trend. Such an offset can be modeled as due to an overall lower rate of supernovae per unit mass in the LMC relative to the Galaxy, as well as a slightly lower ratio of supernovae of Type II to supernovae of Type Ia.

Key words: galaxies: dwarf — Magellanic Clouds

1. INTRODUCTION

The Large Magellanic Cloud (LMC), one of the nearest galaxies and a much smaller system than the Milky Way, is a prime target in which to probe chemical evolution in stellar populations. Unlike the Milky Way, where large fractions of the volume are obscured by dust, the sight lines into most of the LMC are relatively clear, rendering entire populations of stars visible. The LMC's distance demands that detailed stellar abundance studies be based on spectra from 4–8 m class telescopes and be restricted to rather luminous stars.

Pioneering abundance studies have been conducted on LMC stellar samples already. One basic measure of overall chemical evolution in a stellar system is an age-metallicity relation. In the LMC, Olszewski et al. (1991) and Dopita (1996) provide extensive results, with the Olszewski et al. work based on clusters and Dopita's results derived from planetary nebulae. More recently, Geisler et al. (1997) and Bica et al. (1998) have provided additional results from

clusters. A short summary of the LMC age-metallicity relation would note a rapid enrichment phase more than 10 Gyr ago, followed by apparent chemical quiescence until about 2 Gyr ago, when another enrichment period (still ongoing) began.

Additional insights into chemical evolution can be provided by studying elements arising from different nucleosynthetic origins, for example, Type II supernovae (SNe II), Type Ia supernovae (SNe Ia), or asymptotic giant branch stars. Studies of this type require high-resolution spectra and are still a challenging endeavor to undertake in the LMC. Published abundance distributions for the LMC include those of Russell & Dopita (1992), Barbuy, de Freitas Pacheco, & Castro (1994), Hill, Andrievsky, & Spite (1995), Luck et al. (1998), Korn et al. (2000), Hill et al. (2000), Spite et al. (2001), and Korn et al. (2002). The analyzed stars include main-sequence and supergiant B stars, supergiant K to F stars, and Cepheid variables. For the younger stars ($\leq 10^8$ yr), these papers find a typical iron abundance of [Fe/H] ~ -0.3 for LMC field stars. The oxygen-to-iron abundance ratio in the LMC may be measurably lower than this same ratio at the same [Fe/H] abundance in the Galaxy. The trend of [O/Fe] as a function of [Fe/H] can be a crucial relation in establishing star formation histories in a stellar population. Oxygen is made preferentially in the most massive stars, while iron comes from both massive, core-collapse supernovae (SNe II) and the (presumably) binary Type Ia supernovae. The run of the O/Fe ratio with Fe/H in a stellar system is, therefore, a measure of the history of SN II to SN Ia rates and, hence, the star formation history of the LMC. Carbon and nitrogen abundances may also be lower when compared with Galactic stars at the same [Fe/H]. As C, N, and O (with Ne) are the most abundant heavy elements, their abundances carry much weight in setting the overall metallicity, Z, in a galaxy.

Most of the previous abundance determinations of C, N, and O in the LMC have rested on atomic lines, some of which are quite weak, or hampered possibly by non-LTE processes. Because of the importance of the O/Fe ratio to the disentangling of the LMC's star formation history, this study set out to measure oxygen, as well as carbon and nitrogen, abundances in a sample of LMC red giants by observing molecular unblended lines of OH, CO, and CN from high-resolution infrared spectra. Using the 8.3 m Gemini South reflector, along with the Phoenix high-resolution IR spectrometer, abundances of the isotopes ^{12}C, ^{13}C, ^{14}N, and ^{16}O could be determined along with abundances of Fe, Na, Sc, and Ti.

2. OBSERVATIONS AND DATA REDUCTION

High-resolution infrared spectra were obtained of target red giant stars using the 8.3 m Gemini South reflecting telescope and the NOAO[16] Phoenix spectrometer (Hinkle et al. 1998, 2000, 2002). This instrument is a cryogenically cooled echelle spectrograph that uses order-separating filters to isolate individual echelle orders. The detector is a 1024 × 1024 InSb Aladdin II array. The size of the detector in the dispersion direction limits the wavelength coverage in a single

TABLE 1
Program Stars

Star	K	J−K	R.A. (J2000)	Decl. (J2000)
1.6............................	12.60	1.08	05 23 18.93	−69 45 45.5
1.27	10.80	1.26	05 24 00.84	−69 45 44.0
1.50	10.84	1.26	05 23 28.56	−69 48 26.1
2.1158	11.08	1.16	05 31 19.77	−69 58 29.5
2.3256	12.03	1.13	05 32 41.54	−69 53 33.3
2.4525	11.32	1.15	05 31 31.49	−70 04 15.6
2.5368	11.84	1.15	05 30 34.81	−70 02 33.9
HV 2568...................	8.48	1.18	05 29 34.41	−66 55 28.4
NGC 1898 AM 5.......	11.82	1.06	05 16 38.80	−69 39 35.3
NGC 1898 AM 6.......	12.42	0.98	05 16 44.80	−69 39 28.3
NGC 2203 AM 1.......	11.32	1.05	06 04 47.68	−75 25 43.7
NGC 2203 AM 2.......	11.21	1.12	06 04 47.57	−75 25 42.9

Note.—Units of right ascension are hours, minutes, and seconds, and units of declination are degrees, arcminutes, and arcseconds.

exposure to about 0.5% (1550 km s^{-1}, or $\sim$120 Å at 2.3 μm and $\sim$80 Å at 1.6 μm). One edge of the detector is blemished, so the wavelength coverage on all but the brightest sources is typically trimmed a few percent to avoid this area. The InSb material limits the range of sensitivity to the 1–5 μm wavelength region. However, the thermal brilliance of the sky requires that the observation of fainter sources, for example, LMC giants, be limited to the nonthermal 1–2.4 μm region. The spectra discussed here were observed with the widest (0″.35) slit, resulting in a spectral resolution of $R = \lambda/\Delta\lambda = 50,000$.

The program-star positions, K magnitudes, and $J−K$ colors are listed in Table 1. The positions are taken from the Two Micron All Sky Survey (2MASS) database.[17] The first seven stars listed in Table 1 were selected based on a color-magnitude diagram constructed using the 2MASS database for two 15′ fields in the LMC. The LMC red giant branch is clearly visible in a K versus $J−K$ diagram, and all program field giants were found to be LMC members based on their radial velocities. The identifying names given to the field stars here were assigned by us as either field 1 or field 2, followed by the star number from our list for that field, that is, 2.4525 is from field 2 and is number 4525 from that list. In addition to the field stars selected from 2MASS, one star is a bright field supergiant (HV 2568), while four stars in Table 1 were taken from Aaronson & Mould's (1985) IR photometric study of LMC clusters. NGC 1898 AM 5 is found not to be a member of the cluster (as will be seen from our radial velocity and abundance analysis) but a foreground or background LMC giant.

Each program star was observed along the slit at two, three, or four separate positions separated by 5″ on the sky: the delivered image FWHM at the spectrograph varied from 0″.25 to 0″.80 during the nights that spectra were taken, so stellar images at different positions on the slit were well separated on the detector. Equal integration times were used for a particular program star during a particular set of observations. With this observing strategy, sky and dark backgrounds are removed by subtracting one integration from another (the star being at different positions on the

detector array). During each night, 10 flat-field and 10 dark images were recorded for each given wavelength setting of the echelle grating. A hot star, with no intrinsic spectral lines in the regions observed, was also observed each night in each observed wavelength region. If telluric lines were present in the spectral interval, the hot star was observed at air masses bracketing the program stars and suitable combinations of the hot-star spectra were used to divide out the telluric lines from program-star spectra. If no telluric lines fell in the observed region, the hot star was observed only once as a monitor of fringing and general test of data reduction quality. All program stars were observed at two echelle tilts through two different filters: one filter was K4308, with wavelength coverage from 23345 to 23455 Å, and the other was H6420, with wavelength coverage from 15505 to 15575 Å. Table 2 provides an observational log, showing the number and integration time for each observation, as well as the approximate signal-to-noise ratio of each final reduced spectrum (with reduction as described below).

The array image frames were reduced to one-dimensional, wavelength-calibrated spectra with the IRAF[18] set of routines. For a given night and wavelength setting, dark and flat-field frames were averaged and the dark frame was subtracted from the flat field. The average, dark-subtracted flat field was normalized, and the pairs of differenced program-star frames were divided by the normalized flat field. The aperture containing the stellar signal was defined and traced for each star frame, followed by extraction of the spectrum. For the 23400 Å spectra, wavelength calibrations were computed by using a set of telluric wavelengths obtained from the hot-star spectra. In the 15540 Å region, where there are no telluric lines, wavelengths were set using photospheric lines from the red giants themselves, so no radial velocity information can be extracted from the spectra observed in this region. The wavelength calibration fits yielded residuals of typically 0.01–0.02 Å.

Sample reduced spectra are shown in Figure 1 for both spectral regions in one of the field red giants (2.3256). The top panel shows the 15540 Å region and the bottom panel the 23400 Å region. The 23400 Å region contains a number of telluric absorption lines, and this spectrum has been ratioed with the hot star HIP 27603 in order to remove telluric absorption lines. The effective air mass of the telluric
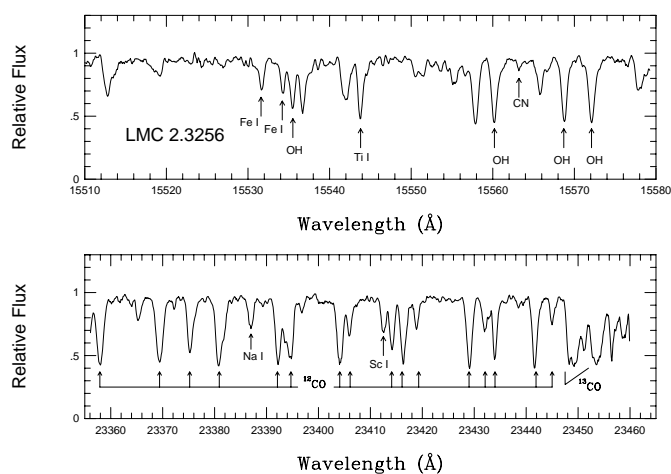

Fig. 1.—Sample spectra of the LMC red giant 2.3256 ($K = 12.0$ mag), with each panel showing a different echelle grating tilt. Some of the stronger lines are identified. Each spectrum consists of a combination of three half-hour integrations, and the signal-to-noise ratio in each spectrum is a bit more than 100 (see Table 2). These spectra are representative of the overall quality of the data analyzed here.

standard star is adjusted by differently weighted averages of the different integrations on this star until the telluric absorption cancels out as well as possible from the program star. In practice, virtually no evidence of such absorption is visible in the program-star spectra. In both regions, a number of the spectral lines or features used in the abundance analysis are identified. This figure illustrates both the quality of the spectra and the variety of lines available for study.

3. ANALYSIS

The analysis uses a combination of photometry and spectroscopy to determine fundamental stellar parameters (effective temperature, surface gravity, microturbulent velocity, and overall stellar metallicity) and detailed chemical compositions. The high-resolution spectra are analyzed using plane-parallel, LTE model atmospheres that are generated using two different versions of the MARCS code: an older version based largely on the program as described by Gustafsson et al. (1975), and a more recent version, OSMARCS (Plez, Brett, & Nordlund 1992; Edvardsson et al. 1993; Asplund et al. 1997), which contains more exten-

TABLE 2
Log of Observations

Star	15540 Å	$(S/N)_{15540}$	23400 Å	$(S/N)_{23400}$
1.6............................	2001 Dec 21: 3 × 1200 s	65	2002 Feb 4: 4 × 1800 s	95
1.27..........................	2001 Dec 21: 2 × 1800 s	155	2002 Feb 2: 3 × 600 s	105
1.50..........................	2002 Feb 5: 4 × 600 s	150	2002 Feb 2: 3 × 600 s	120
2.1158	2002 Feb 5: 3 × 1200 s	200	2002 Feb 3: 3 × 1200 s	225
2.3256	2002 Feb 7: 3 × 1800 s	105	2002 Feb 3: 3 × 1800 s	115
2.4525	2002 Feb 5: 3 × 900 s	90	2002 Feb 4: 3 × 1200 s	100
2.5368	2002 Feb 5: 3 × 1800 s	75	2002 Feb 3: 3 × 1800 s	125
HV 2586....................	2001 Dec 21: 2 × 600 s	210	2001 Dec 23: 4 × 600 s	220
NGC 1898 AM 5.......	2002 Feb 6: 3 × 1800 s	70	2002 Feb 9: 3 × 1200 s	105
NGC 1898 AM 6.......	2002 Feb 6: 3 × 1800 s	50	2002 Feb 9: 3 × 1800 s	95
NGC 2203 AM 1.......	2001 Dec 21: 4 × 1200 s	125	2002 Feb 2: 3 × 1200 s	115
NGC 2203 AM 2.......	2001 Dec 21: 4 × 1200 s	80	2002 Feb 2: 3 × 1200 s	80

sive molecular opacities. Abundances derived from both types of models are compared to give some indication of potential model atmosphere systematic effects. The model atmospheres are coupled to the most recent version of the LTE spectrum synthesis code MOOG (Sneden 1973) in order to derive abundances.

3.1. Stellar Effective Temperatures

The effective temperatures of the stars are chosen using broadband color $(J-K)$-$T_{\rm eff}$ calibrations. Table 1 listed the stars observed along with their K magnitudes and $J-K$ colors. The 2MASS database is the source of the magnitudes and colors for the field giants, while Aaronson & Mould (1985) was used for the cluster members. The 2MASS magnitudes and colors have been transformed to the system defined by Bessell & Brett (1988), as we use $T_{\rm eff}$ calibrations from Bessell, Castelli, & Plez (1998), who use the color system defined in Bessell & Brett (1988). The 2MASS corrections are those defined by Carpenter (2001) in his Appendix A and are fairly small: a constant 0.04 mag offset in K, and a small color term that is about 0.03 mag in $J-K$. Table 3 lists the absolute bolometric magnitudes based on a distance modulus of 18.5 and K-band bolometric corrections from Bessell et al. (1998): no corrections for reddening in the IR were included here.

Bessell et al. (1998) show that $T_{\rm eff}$-$(J-K)$ relations have a small metallicity dependence, and we use their calibration for [Fe/H] = -0.50, which is what is expected for the typical LMC field (Cole, Smecker-Hane, & Gallagher 2000): Table 3 lists these effective temperatures. Other color–effective temperature relations are available in the literature. We compare one other source (McWilliam 1990) with the calibrations used here. The mean difference between the effective temperatures from the Bessell et al. (1998) calibration minus those from the McWilliam (1990) calibration is $+90 \pm 51$ K, suggesting that the temperature scale may be accurate to about 100 K.

3.2. Surface Gravities, Microturbulent Velocities, and Iron Abundances

The stellar surface gravity can usually be derived from either ionization equilibria (where, e.g., Fe I and Fe II lines are forced to yield the same abundance) or from estimates of stellar luminosity and mass. No ionized atomic lines are detectable in the relatively small IR spectral windows

observed here, so gravities are defined by luminosity and mass estimates from the standard relation

$$g/g_\odot = \left(\frac{M}{1\,M_\odot} \right) \left(\frac{T_{\rm eff}}{T_{\rm eff,\odot}} \right)^4 \left(\frac{1\,L_\odot}{L} \right).$$

For LMC red giants, bolometric magnitudes (Table 3) and, hence, absolute luminosities are known with some accuracy; the distance modulus adopted is 18.5 ± 0.2. Mass estimates are obtained using evolutionary tracks. Figure 2 shows plots of $M_{\rm bol}$ versus $T_{\rm eff}$ for the LMC red giants from this work and model tracks from Schaerer et al. (1993), with the model tracks computed for the metallicity expected for most of the LMC program stars ([Fe/H] = -0.35). Models are shown for 1.0, 2.0, 3.0, 4.0, 5.0, 7.0, and 10.0 $M_\odot$, and these tracks stop at the tip of the first ascent of the red giant branch (RGB). A. Karakas & J. Lattanzio (2002, private communication) kindly provided tracks for 1.0, 1.9, 3.0, and 4.0 $M_\odot$ models that included evolution along the asymptotic giant branch (AGB) and into the thermally pulsing (TP-AGB) phase of evolution (with these models also computed for an LMC metallicity). The two separate sets of models from Schaerer et al. and Karakas & Lattanzio agree well from evolution on the zero-age main sequence and onto the RGB; on the AGB and TP-AGB the tracks become rather complicated, and these tracks are not plotted in Figure 2, for the sake of clarity.

The top panel of Figure 2 provides a broad view of stellar evolution and includes the positions of a few other samples of LMC stars from previously published abundance studies, whose results will be compared with those derived here. Korn et al. (2002) is an analysis of four main-sequence B star members of the young cluster NGC 2004, while Korn et al. (2000) studies five somewhat evolved B star members in two clusters (NGC 2004 again and NGC 1818). Hill et al. (1995) derived abundances in nine field nonvariable (or very slightly variable) F supergiants. What Figure 2 makes clear is that compared with these earlier LMC studies, the stars sampled here are of rather lower mass. The earlier abundances mentioned above are derived from LMC stars with masses of $\sim$10 $M_\odot$, while the red giants analyzed here have masses closer to $\sim$2–4 $M_\odot$. The mass and evolutionary regimes are quite different, and thus our study can add complementary abundance information to what has been derived already for the LMC.

TABLE 3
DERIVED STELLAR PARAMETERS

| Star	$M_{\rm bol}$	$T_{\rm eff}$ (K)	Mass ($M_\odot$)	$\log g$ (cm s^{-2})	ξ (km s^{-1})	[Fe/H]	V_r (km s^{-1})
1.6............................	-3.18	3760	2	$+0.8$	2.5	-0.50	$+262.0 \pm 0.3$
1.27..........................	-4.77	3550	3	$+0.3$	3.1	-0.36	$+246.0 \pm 0.5$
1.50..........................	-4.73	3550	3	$+0.3$	2.8	-0.37	$+263.9 \pm 0.8$
2.1158	-4.60	3640	3	$+0.4$	2.5	-0.34	$+281.6 \pm 0.5$
2.3256	-3.69	3680	2	$+0.6$	2.6	-0.45	$+229.8 \pm 0.4$
2.4525	-4.37	3650	3	$+0.5$	3.0	-0.45	$+251.4 \pm 0.4$
2.5368	-3.85	3650	2	$+0.5$	1.9	-0.38	$+232.2 \pm 0.5$
HV 2586....................	-7.18	3600	10	-0.1	3.5	-0.52	$+289.6 \pm 1.2$
NGC 1898 AM 5.......	-3.98	3810	3	$+0.7$	2.2	-0.50	$+254.7 \pm 0.4$
NGC 1898 AM 6.......	-3.49	3970	1	$+0.5$	3.2	-1.13	$+219.3 \pm 0.3$
NGC 2203 AM 1.......	-4.23	3850	3	$+0.6$	3.3	-0.67	$+253.4 \pm 0.6$
NGC 2203 AM 2.......	-4.51	3700	3	$+0.4$	3.1	-0.61	$+253.1 \pm 0.8$
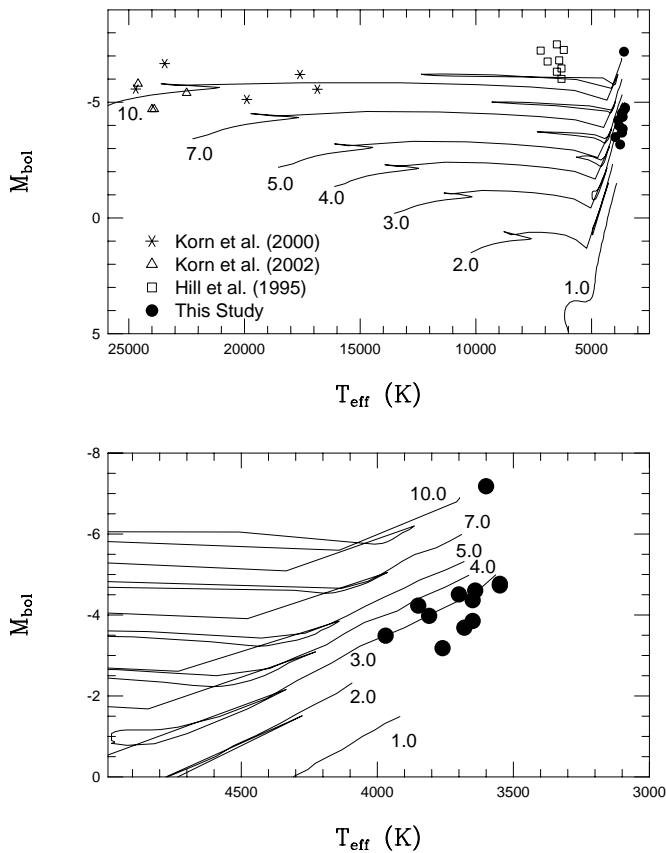
Fig. 2.—Modified Hertzsprung-Russell diagrams, with absolute bolometric magnitude vs. effective temperature, for the red giants analyzed here, a few other LMC stellar samples with published abundances, and stellar model tracks from Schaerer et al. (1993). Note that previous LMC stellar abundance analyses tended to sample the more massive stars, while the red giants presented here have lower masses. The bottom panel shows an expanded view of the red giant region, with the model tracks terminated at the tip of the red giant branch. Models of AGB stars were computed by A. Karakas & J. Lattanzio (2002, private communication); however, their tracks are complex and are not plotted here for clarity. The AGB tracks confirm that the red giants in this sample are either first-ascent stars or early AGB stars. Mass estimates for these LMC giants are based on the Schaerer et al. tracks and span a narrow range of $\sim 2-4\ M_\odot$, except for the massive supergiant HV 2586 and the lower mass metal-poor giant NGC 1898 AM 6.

The bottom panel of Figure 2 shows, in more detail, the exact location of the target stars from this study. Except for the massive supergiant, HV 2586, the red giants fall in a narrow region crossed by either first-ascent giants, or early AGB stars with masses in the range of $\sim 2-4\ M_\odot$. Individual masses were estimated for each LMC red giant, and these approximate masses are listed in Table 3: these masses were obtained by comparisons with both the Schaerer et al. and Karakas & Lattanzio tracks. The star NGC 1898 AM 6 is worth a special note, as it will turn out to be significantly more metal-poor than the other stars in this sample (with [Fe/H] = -1.13). Model tracks with [Fe/H] = -0.35, at a given mass, are too red for this giant, and more appropriate tracks indicate that it is a lower mass giant with $M \sim 1.0\ M_\odot$. The surface gravities used for the abundance analysis were then calculated from the mass estimates and are listed in Table 3, rounded to the nearest solar mass. Since no program star, except the obviously massive supergiant HV 2586, appears likely to be above 4 $M_\odot$, and none apparently

at masses lower than 2 $M_\odot$ (except for the metal-poor cluster member NGC 1898 AM 6), it is likely that errors in the surface gravity do not exceed ~ 0.2 dex, which would not cause a significant error in derived abundances.

Modeling the behavior of spectral lines with one-dimensional model atmospheres requires the definition of the microturbulent velocity ξ. The value of ξ is set by the condition that lines of differing line strengths from the same species result in the same abundances. In the IR spectral windows observed here, the numerous $^{12}C^{16}O$ (hereafter ^{12}CO) lines in the 23400 Å window can be used, as the various rotational lines from the 3–1 vibration series exhibit a variety of line strengths (see Fig. 1). The detailed selection of the ^{12}CO lines is discussed in § 3.4, but Figure 3 shows an example of the determination of the microturbulent velocity for the cluster member red giant NGC 2203 AM 1. The left panels show values of slopes versus ξ for the abundance versus reduced equivalent widths (top) and abundance versus excitation potential slopes (bottom). Both plots show a zero slope at nearly the same value of the microturbulence, indicating that the T_{eff} used for this star is a reasonably good value, as the abundance versus excitation potential is sensitive to the temperature; thus, a unique value of ξ provides a simultaneous fit to both line strength and excitation potential. The right panels illustrate the quality of the spectral line data by showing the derived abundances versus both reduced equivalent width (top) and versus excitation potential (bottom) for the best-fit value of $\xi = 3.3$ km s^{-1}. Both trends show effectively zero slopes and small scatter (± 0.05 dex in the ^{12}C abundance). The derived microturbulent velocities are listed in Table 3.

The right panels in Figure 3 also illustrate an experiment conducted on line formation in the model atmospheres. The ^{12}CO lines are formed over a range of optical depths in the atmosphere, with strong lines being formed preferentially higher compared with weaker lines. The circles in these panels show results for a "standard" model atmosphere used in the abundance analysis: standard here means the atmosphere extends to optical depths, defined at $\lambda = 5000$ Å as low as $\tau_{5000} = 10^{-4}$, at which point the atmosphere is truncated. The squares show abundances from the ^{12}CO lines for a model that has been truncated at $\tau_{5000} = 10^{-3}$; as some of the ^{12}CO lines are the strongest lines in the spectra, if substantial contributions to their absorption were occurring near $\tau_{5000} \sim 10^{-4}$, truncating the models here would result in incorrect abundances. Clearly, truncating at either 10^{-3} or 10^{-4} in optical depth has no significant effect ($\leq 0.01-0.02$ dex) on derived abundances, and the optical depth structures of the models are adequate.

Earlier abundance studies of Galactic red giants that overlap somewhat the effective temperatures and gravities of the stars studied here were Smith & Lambert (1985, 1986, 1990), and it is instructive to compare values of the microturbulence derived from those papers and the microturbulent velocities measured here; the Smith & Lambert analyses relied on near-IR Fe I lines as the primary indicators with which to set ξ, while using the ^{12}CO lines as secondary checks. The top panel of Figure 4 is a plot of ξ versus absolute bolometric magnitude for the LMC red giants and the Galactic stars from the Smith & Lambert papers. It appears that the lower luminosity giants have a typical $\xi = 2.0$ km s^{-1}, but at luminosities greater than $M_{bol} \sim -2.5$ there is a trend of increasing values of ξ with increasing absolute magnitude, as well as increasing amounts of scatter. The LMC
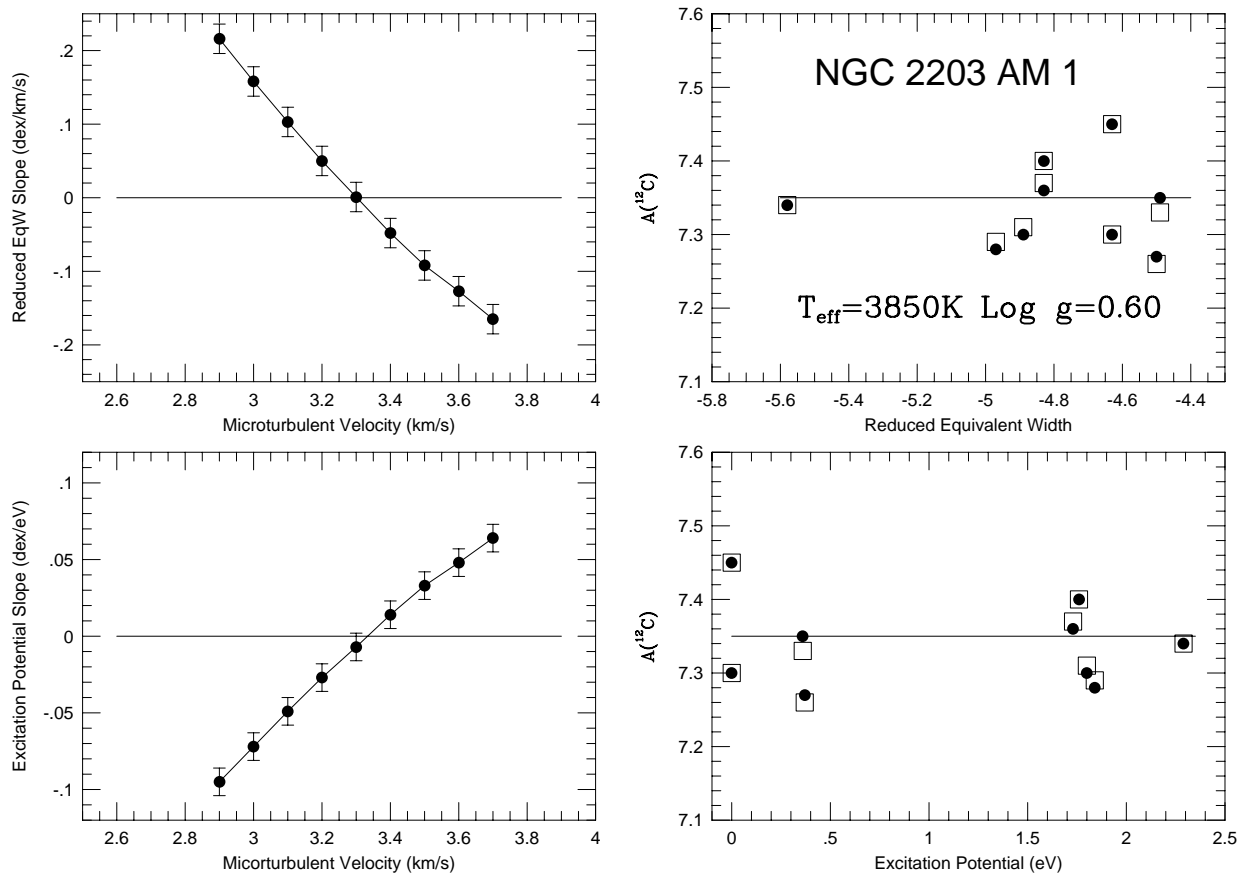
Fig. 3.—Illustration of the determination of the microturbulent velocity ξ for one red giant (AM 1 in NGC 2203). The left panels show the linear slopes resulting from fits to the carbon abundances (derived from CO lines) vs. reduced equivalent width (*top*) and vs. excitation potential (*bottom*) for various microturbulent velocities. No trend, i.e., zero slope, for both reduced equivalent width and excitation potential signifies a best fit. The effective temperature was set by IR colors; note that a single value of ξ also results in a zero slope with excitation potential (which is most sensitive to $T_{\rm eff}$). The simultaneous solutions for both reduced equivalent width and excitation potential indicate a satisfactory fit for both $T_{\rm eff}$ and ξ. The right panels show the quality of the abundances for the given $T_{\rm eff}$–ξ solution (a scatter of about ± 0.06 dex) for this star. The circles result from a model atmosphere extending to an optical depth at 5000 Å of $\tau = 10^{-4}$ (what we usually use as the upper atmospheric cutoff), while the squares are the abundances resulting from truncating the atmosphere at $\tau = 10^{-3}$. As some of the ^{12}CO lines are the strongest ones used, their insensitivity to model atmosphere details in the regime $\tau = 10^{-3}$–10^{-4} indicates that the atmospheric structure is adequate for this abundance analysis.

red giants fall right within the scatter as defined by the Galactic giants, with the LMC sample tending to be composed of stars of slightly higher luminosities than the samples of Galactic stars studied by Smith & Lambert (1985, 1986, 1990) but exhibiting the same basic behavior in terms of the microturbulence. The bottom panel of Figure 4 is in a similar vein to the top panel: here ξ is plotted versus log g. Microturbulent velocities for the Milky Way giants cluster around 2.0 km s^{-1} for the higher gravity stars (log $g \geq 1.0$), but then ξ increases both in magnitude and scatter as gravity decreases. The overlap between Galactic and LMC giants is essentially perfect.

The metallicity is estimated from the 15540 Å window, where three Fe I lines are measurable as largely unblended features. The next section covers the line-list selections for the various species in detail, but the [Fe/H] values listed in Table 3 are from these three lines, using gf-values set by fits to the IR Arcturus spectral atlas (Hinkle, Wallace, & Livingston 1995) using the Fe abundance determined from optical Fe I and Fe II lines (Smith et al. 2000). The parameters for α Boo (Arcturus) adopted here are those derived by Smith et al. (2000): $T_{\rm eff} = 4300$ K, log $g = 1.7$, $\xi = 1.6$ km s^{-1}, and [Fe/H] = -0.72.

The last column of Table 3 lists the heliocentric radial velocities of the program stars as determined from the sample of nine ^{12}CO lines used to set the microturbulence. From the radial velocities it is found that all program stars are LMC members; Prévot et al. (1985) found velocities of field stars in the LMC to range from about $+250$ to $+310$ km s^{-1}. The two clusters in our sample were also observed by Olszewski et al. (1991) for both radial velocities and metallicities (not the same stars as observed here, however). In the case of NGC 2203, Olszewski et al. find a mean radial velocity of $+243$ km s^{-1}, which is close to the $+253$ km s^{-1} found for the two member stars in this sample. They also derive a cluster metallicity of [Fe/H] = -0.53, a value similar to what we find for AM 1 (-0.67) and AM 2 (-0.61). For NGC 1898, Olszewski et al. observe a mean cluster velocity of $+210$ km s^{-1} and a metallicity of [Fe/H] = -1.37. This radial velocity and abundance are close to what we find for AM 6 ($V = +219$ km s^{-1} and [Fe/H] = -1.1). For the other star, AM 5, we find $V = +255$ km s^{-1} and [Fe/H] = -0.50, quite different from Olszewski et al. (1991) or what we find for AM 6. This star is almost certainly a cluster nonmember; however, its velocity indicates that it is a member of the LMC. It is either a fore-
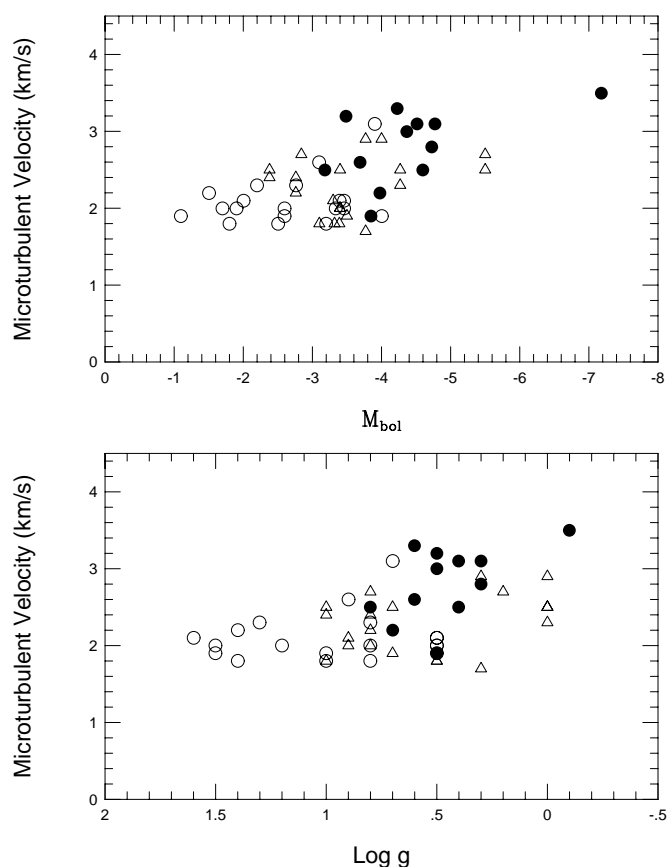
Fig. 4.—Microturbulent velocities, as determined for Galactic M giants (*open circles*), or MS and S stars (*triangles*), from Smith & Lambert (1985, 1986, 1990), and the LMC red giants (*filled circles*) vs. absolute bolometric magnitude (*top*) and logarithm of the surface gravity (*bottom*). The overlap in ξ with both M_{bol} and log g between the Galactic giants and the LMC giants is excellent. At lower luminosity (with $M_{bol} \geq -3$) and larger log g (≥ 1), there is an almost constant microturbulence of $\xi \sim 2.0$–2.5 km s^{-1}. As luminosity increases and surface gravity decreases, ξ increases slowly toward 3.0–3.5 km s^{-1}, with the Galactic and LMC giants following a similar trend.

ground or background LMC red giant in the field of NGC 1898.

3.3. *The Atomic Lines Used:* Fe I, Na I, Sc I, *and* Ti I

In the two spectral intervals sampled, a handful of atomic lines are detectable that are largely unblended and single. These lines are listed in Table 4, along with the measured equivalent widths from the 12 program LMC red giants. The excitation energies are from the Kurucz & Bell (1995) lists, while the *gf*-values have been adjusted to provide the same abundances from these lines in α Boo (Hinkle et al. 1995) as found from the analysis of this standard star in conjunction with analyses of ω Cen red giants (Smith et al. 2000). Table 4 lists the line data and equivalent widths for all 12 of the program stars.

3.4. *The Molecular Lines Used for the* CNO *Abundances:* CO, OH, *and* CN

The IR windows were chosen to provide molecular lines from which to derive the C, N, and O abundances. The 23400 Å region includes lines of the CO first-overtone vibration-rotation bands. The 15540 Å region includes lines of the OH first-overtone vibration-rotation bands and the CN

red system. Partial pressures of C and O are coupled through the formation of CO and, to a lesser extent, of OH and H_2O. The partial pressure of N is controlled almost exclusively by formation of N_2. Minor influences of other molecules was taken fully into account. A simultaneous analysis of CO and OH lines provides the C and O elemental abundances. Analysis of the CN lines and the C abundance give the N abundance.

The wavelengths, excitation potentials, and *gf*-values for the CO vibration-rotation lines are from Goorvitch (1994), with the $\Delta v = 2$ lines in the 23400 Å region being used. The ^{12}CO lines measured span a range in line strength and χ and were used to set the microturbulence, as well as to provide a check on the adopted T_{eff} from the $J-K$ photometry. The CO dissociation energy was taken as $D_0 = 11.090$ eV. In addition to the ^{12}CO lines, the ^{13}CO (2–0) band head falls at the red edge of the 23400 Å setting in all but one program star, and synthesis of this band head was used to derive a ^{13}C abundance (tabulated as a ^{12}C/^{13}C ratio).

The spectral region near 15540 Å was selected because it contains a number of relatively isolated and unblended OH lines, as used in previous oxygen analyses by Balachandran & Carney (1996), Meléndez, Barbuy, & Spite (2001), and Meléndez & Barbuy (2002). Asplund & García Pérez (2001) have pointed out that strong OH lines may be sensitive to the effects of temperature differences and granulation that are found in the three-dimensional model atmospheres but not in the one-dimensional models; however, their calculations covered effective temperatures that are considerably hotter ($T_{eff} = 5800$–6200 K) than those found here. Nissen et al. (2002) point out that the granulation effects on the OH lines from the three-dimensional models are expected to decline with decreasing effective temperature. Meléndez & Barbuy (2002) confirmed that oxygen abundances derived from the stronger lines are higher than for the weaker OH lines, again, however, for stars that are distinctly hotter than those sampled here. The differences found by Meléndez & Barbuy are more pronounced for more metal-poor stars and disappear for stars with [Fe/H] ≥ -1. The combination of lower effective temperatures and higher metallicities in the stars sampled here is why this effect is not found in our oxygen abundances. The wavelengths, excitation potentials, and *gf*-values are from Goldman et al. (1998), with the dissociation energy being $D_0 = 4.392$ eV (Huber & Herzberg 1979).

Nitrogen abundances are based on five CN lines in the 15540 Å spectral region (these CN lines are weaker than the CO and OH lines but are well defined and typically unblended). The CN lines were chosen from a line list extracted from a master list compiled by B. P. as described in Hill et al. (2002). The CN dissociation energy is $D_0 = 7.77$ eV (Costes, Naulin, & Dorthe 1990).

The molecular line data, as well as the measured equivalent widths, are listed in Table 4.

3.5. *Errors from Stellar Parameter Uncertainties and Final Abundances*

As already discussed in § 3.1, uncertainties exist in T_{eff} of at least ~100 K and gravities may be uncertain by about ± 0.2 dex. Fits to the ^{12}CO lines to determine ξ constrain this parameter to ± 0.2–0.3 km s^{-1}. In order to investigate how these parameter uncertainties manifest themselves as abundance changes, the model for the program star 2.4525,

TABLE 4
SPECTRAL LINE DATA AND EQUIVALENT WIDTHS

λ (Å)	χ (eV)	log gf	LMC 1.6	LMC 1.27	LMC 1.50	LMC 2.1158	LMC 2.3256	LMC 2.4525	LMC 2.5368	HV 2586	NGC 1898 AM 5	NGC 1898 AM 6	NGC 2203 AM 1	NGC 2203 AM 2
Fe I:														
15531.742	5.64	−0.564	141	182	171	189	169	178	146	214	175	...	170	198
15534.239	5.64	−0.402	253	275	253	290	174	211	208	230	176	128	244	195
15537.572	5.79	−0.799	106	169	105	142	83	136	79	125	58	41	116	90
Na I:														
23378.945	3.75	−0.420	376	418	427	476	277	402	398	294	322	95	364	442
Sc I:														
23404.756	1.44	−1.278	213	617	496	327	321	472	354	602	240	74	476	668
Ti I:														
15543.720	1.88	−1.481	382	482	427	428	327	442	353	415	345	188	532	452
$^{12}C^{14}N$:														
15530.987	0.89	−1.519	108	163	197	150	47	...	...	...	48	...	120	126
15544.501	1.15	−1.146	67	142	111	84	81	87	65	181	47	...	99	78
15552.747	0.90	−1.680	...	127	112	85	48	23	38	...	20	25	78	...
15553.659	1.08	−1.285	30	143	123	115	72	81	78	160	37	...	97	93
15563.376	1.15	−1.141	85	130	140	122	46	68	78	182	64	...	95	102
$^{12}C^{16}O$:														
23396.305	0.37	−5.167	611	869	933	781	736	741	555	1033	543	485	732	837
23398.275	1.73	−4.438	310	391	390	359	308	334	316	420	374	96	349	431
23406.389	0.00	−6.565	482	648	794	531	444	535	526	612	436	312	573	635
23408.555	0.36	−5.190	640	771	855	657	668	772	620	1119	604	426	755	866
23411.070	1.76	−4.430	212	419	442	344	321	282	293	580	406	80	348	334
23424.328	1.80	−4.427	255	287	262	273	303	279	280	329	183	92	304	211
23426.322	0.00	−6.744	418	511	549	461	482	528	398	...	615	177	550	541
23431.240	2.29	−4.757	77	136	110	80	61	85	95	...	120	56	62	50
23438.059	1.84	−4.414	214	299	309	230	162	261	230	300	315	39	250	181
^{16}OH:														
15535.489	0.51	−5.233	277	398	392	277	300	340	261	327	213	228	388	326
15560.271	0.30	−5.307	246	527	525	415	392	491	374	366	367	286	518	421
15568.807	0.30	−5.270	243	517	470	340	396	463	372	372	312	315	500	405
15572.111	0.30	−5.270	291	505	466	363	442	463	384	387	313	295	477	398

NOTE.—Equivalent widths in milliangstroms.

which has an effective temperature near the middle of the program-star distribution, was perturbed by +100 K in T_{eff}, +0.2 dex in log g, and +0.2 km s^{-1}, respectively, and abundances computed for each perturbation. These abundance changes are listed in Table 5 for each species used in the abundance analysis. These changes can be assumed to be quasi-linear for small changes in the stellar parameters across the range of values found for this sample of red giants and be used to assess the overall uncertainties in the abundance analysis.

Systematic effects are always possible, for example, due to the choice of type of model atmosphere. This possibility was investigated by comparing abundances derived from two different sets of model atmospheres, one from the older MARCS program and the other from the newer OSMARCS code. In none of the stellar parameters spanned by the program stars was it found that derived abundance differences exceeded 0.10 dex. In the deeper layers (where $\tau_{5000} \geq 0.6$), the two sets of models agree in temperature and pressure. In regions where spectral lines form (typically $\tau_{5000} \sim 0.1$), differences are still essentially zero at $T_{eff} = 3800$ K, but the OSMARCS models become slightly warmer (by about 40 K) and have higher gas pressures (by about 20%) for $T_{eff} = 3600$ K. The lines affected most by the differing models at this effective temperature were from OH (note the temperature sensitivity

TABLE 5
SENSITIVITY OF ABUNDANCES TO STELLAR PARAMETERS

Element	$\Delta T_{eff} = +100$ K	Δ log $g = +0.2$	$\Delta\xi = +0.2$ km s^{-1}	Δ_{tot}
ΔFe	−0.10	+0.05	−0.04	0.12
ΔC	+0.05	−0.15	−0.06	0.17
ΔN	−0.11	+0.18	−0.01	0.21
ΔO	+0.22	+0.01	−0.09	0.24
ΔNa	+0.09	−0.04	−0.04	0.11
ΔSc	+0.19	−0.02	−0.06	0.20
ΔTi....................	+0.16	+0.00	−0.08	0.18

TABLE 6
Abundances

Star	$A(\text{Fe})$	$A(^{12}\text{C})$	$^{12}\text{C}/^{13}\text{C}$	$A(^{14}\text{N})$	$A(^{16}\text{O})$	$A(\text{Na})$	$A(\text{Sc})$	$A(\text{Ti})$
1.6..........................	7.00 ± 0.10	7.52 ± 0.11	11 ± 3	7.57 ± 0.15	8.02 ± 0.17	5.65	2.49	4.55
1.27........................	7.14 ± 0.13	7.39 ± 0.16	...	8.14 ± 0.09	8.24 ± 0.11	5.60	2.80	4.31
1.50........................	7.13 ± 0.05	7.49 ± 0.08	16 ± 3	8.24 ± 0.11	8.29 ± 0.15	5.55	2.72	4.39
2.1158	7.16 ± 0.06	7.38 ± 0.14	21 ± 4	8.12 ± 0.16	8.11 ± 0.15	5.68	2.61	4.44
2.3256	7.05 ± 0.09	7.50 ± 0.10	12 ± 3	7.73 ± 0.16	8.22 ± 0.09	5.34	2.61	4.15
2.4525	7.05 ± 0.10	7.34 ± 0.13	10 ± 3	7.72 ± 0.18	8.29 ± 0.13	5.38	2.80	4.24
2.5368	7.12 ± 0.10	7.57 ± 0.10	7.5 ± 1.5	7.77 ± 0.13	8.26 ± 0.15	5.80	2.65	4.61
HV 2586...................	6.98 ± 0.09	7.27 ± 0.13	35 ± 6	7.91 ± 0.05	7.87 ± 0.15	5.84	2.50	4.19
NGC 1898 AM 5.......	7.00 ± 0.12	7.86 ± 0.15	20 ± 4	7.14 ± 0.15	8.33 ± 0.16	5.71	2.60	4.54
NGC 1898 AM 6.......	6.37 ± 0.05	6.53 ± 0.09	3.5 ± 1.5	...	7.82 ± 0.08	4.69	2.01	3.84
NGC 2203 AM 1.......	6.83 ± 0.11	7.35 ± 0.08	19 ± 4	8.15 ± 0.13	8.31 ± 0.13	5.25	2.85	4.27
NGC 2203 AM 2.......	6.89 ± 0.07	7.42 ± 0.06	45 ± 10	7.99 ± 0.08	8.20 ± 0.14	5.57	2.91	4.30
Sun	7.50	8.59	89	8.00	8.77	6.33	3.17	5.02
α Boo........................	6.78	7.79 ± 0.08	8.0 ± 1.0	7.65 ± 0.07	8.39 ± 0.05	5.85	2.64	4.64

Note.—Where $A(\text{X}) = \log [n(\text{X})/n(\text{H})] + 12$.

in Table 5); however, the effects were small and of no significant consequence to the abundances reported here.

Final abundances, based on the OSMARCS models, are listed in Table 6 in the $A(\text{X}) = \log \epsilon(\text{X}) = \log [n(\text{X})/n(\text{H})] + 12$ system. The ^{13}C abundances are reported in the traditional form of ^{12}C-to-^{13}C ratios. For species with abundances derived from three or more lines, the standard deviation of the mean is also shown: this provides some rough estimate of the quality of the spectra used in the analysis. All abundances were based ultimately on spectrum synthesis, although the equivalent widths listed in Table 4 were used for a first-cut abundance analysis. Included in Table 6 are the adopted abundances in the Sun for the elements studied, as well as for the well-studied, metal-poor red giant α Boo. The α Boo abundances for Fe, Na, Sc, and Ti are those from Smith et al. (2000); the atomic line gf-values were adjusted so as to yield these abundances in α Boo from an analysis of these lines in the Infrared Atlas spectrum of this star (Hinkle et al. 1995). The abundances in α Boo for C, N, and O (including ^{13}C) were derived from the same spectral regions and lines of CO, OH, and CN as used in the analysis of the LMC program stars.

Examples of two spectral syntheses in LMC red giants are shown in Figure 5. The top panel shows one region containing three ^{12}CO lines (of differing strengths) and an Sc I line. The spectrum displayed is that from LMC 1.6, and three separate ^{12}C and Sc abundances are illustrated in the syntheses. The comparisons between observed and model spectra are excellent. The bottom panel shows two of the OH lines in NGC 1898 AM 6 with, again, three different oxygen abundances in the synthetic spectra. Examples of observed and synthetic spectra of the blended ^{13}CO (2–0) band head are displayed in Figure 6. The top panel shows the LMC field giant 2.1158, which has an estimated mass of $\sim 3\ M_\odot$ (Fig. 2 and Table 3). Syntheses with three different isotopic carbon ratios are shown, with $^{12}\text{C}/^{13}\text{C} = 17$ providing the best fit. The cluster member AM 6 of NGC 1898 is shown in the bottom panel to illustrate ^{13}CO in a lower mass ($\sim 1\ M_\odot$), lower metallicity ([Fe/H] = -1.1) giant. In this star, a much lower isotopic ratio is derived, with $^{12}\text{C}/^{13}\text{C} = 3.5$.

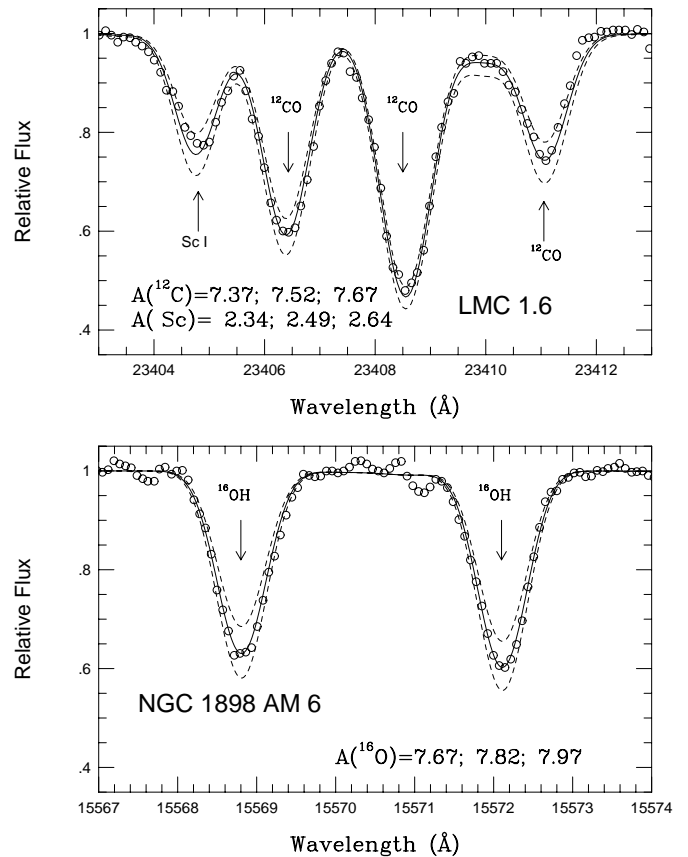
Fig. 5.—Sample synthetic and real spectra in two spectral regions in two different stars. The top panel illustrates a small spectral region in the K band showing three ^{12}CO lines, of differing strengths, and an atomic Sc I line. The circles are the observed data, while the curves are synthetic spectra with differing carbon and scandium abundances (as shown in the figure). Note that the three ^{12}CO lines, with very different equivalent widths and excitation potentials, yield nearly the same ^{12}C abundance. The bottom panel shows two OH lines in the H band, again with the circles being the real spectrum and the curves showing synthetic spectra with differing ^{16}O abundances.
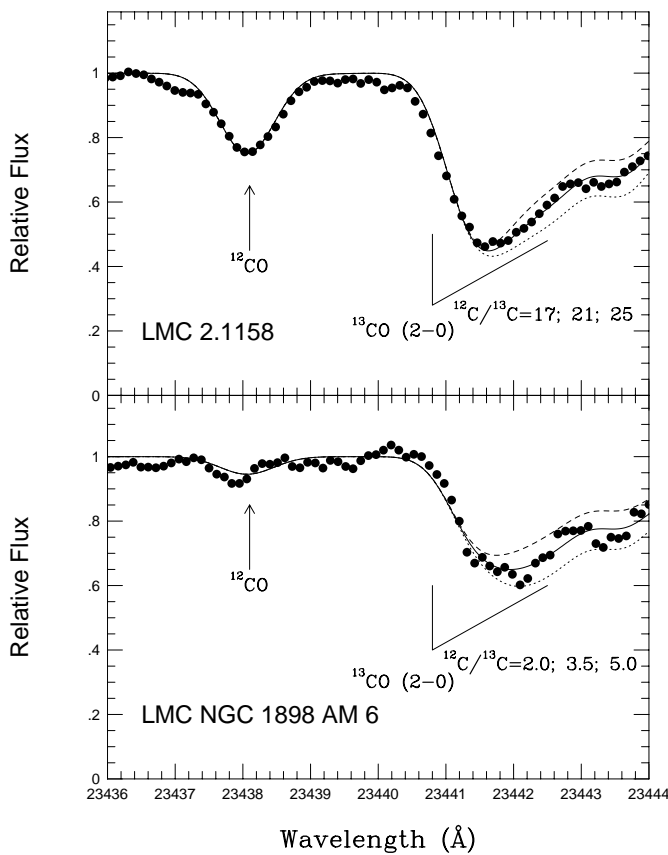
FIG. 6.—Examples of synthetic spectral fits to the blended ^{13}CO (2–0) band head in two LMC red giants. The top panel shows a field star (2.1158) that has an estimated mass of 3 $M_\odot$, with a metallicity of [Fe/H] $= -0.34$, and having a fairly large $^{12}C/^{13}C$ ratio, typical of the slightly higher mass red giants in this sample. The bottom panel illustrates the ^{13}CO band head in the most metal-poor star in the sample, the cluster member AM 6 in NGC 1898, with [Fe/H] $= -1.13$. This is an old LMC red giant, with an estimated mass of 1 $M_\odot$ and a low isotopic ratio ($^{12}C/^{13}C = 3.5$); the trend in the LMC of lower carbon isotope ratios with lower mass and metallicity is in the same sense as in the Milky Way.
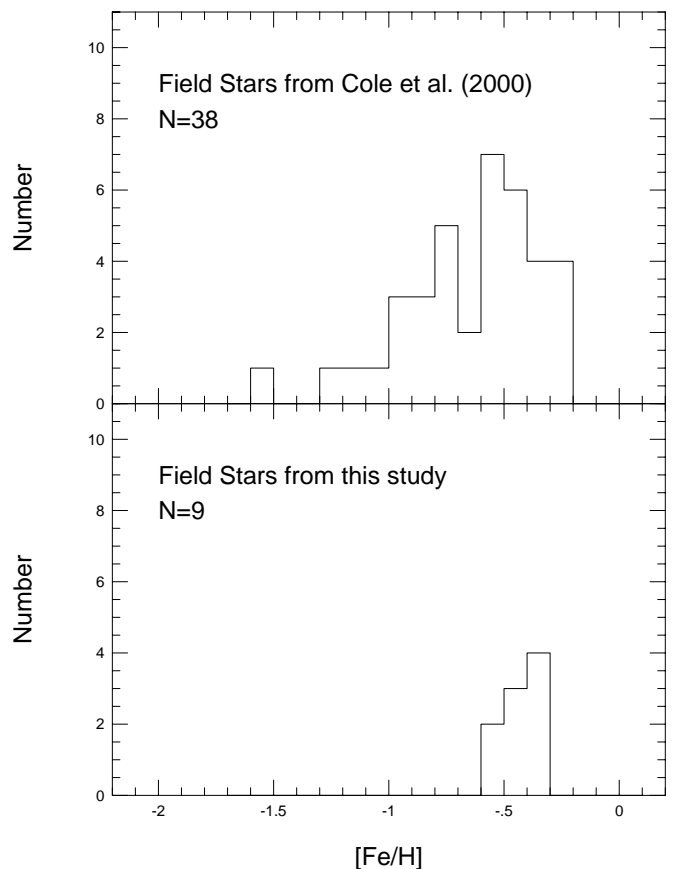

FIG. 7.—Comparison of field star iron abundances from the large study by Cole et al. (2000, top) and for the field LMC red giants analyzed here. The Cole et al. results are derived from low-resolution spectra of the Ca II IR triplet, while [Fe/H] for the stars here are from three Fe I lines in the H band. Our current sample of nine field stars is too small to compare with the shape of the metallicity distribution as defined by the Cole et al. (2000) sample; however, the average [Fe/H] of our sample agrees very well with that expected from the Cole et al. distribution.

4. DISCUSSION

Observational understanding of a stellar system's chemical evolution must pursue a selection of elements whose stellar surface abundances are considered to reflect faithfully the composition of the gas from which the stars formed. Here Na, Sc, Ti, and Fe may plausibly be deemed such a selection. Below, we discuss some implications of our abundances, primarily by contrasting abundance ratios relative to Fe in the LMC, the Galaxy, and other systems.

On the other hand, surface abundances of C and N in red giants are well recognized to be affected by convective mixing. This mixing rearranges the C and N abundances and obscures the original abundances that betray the chemical evolution of the stellar system. We compare C and N in LMC and Galactic red giants.

Oxygen is likely unaffected by the convective mixing until the giant evolves to the asymptotic giant branch. Here we assume that O is a probe of chemical evolution and discuss the O/Fe ratio in the LMC and the Galaxy.

4.1. The LMC Iron Abundances

The red giant sample here consists of nine stars that are not associated with any clusters and are thus categorized as field stars, and three stars that are members of clusters (one in NGC 1898 and two in NGC 2203). Recently, Cole et al. (2000) have begun to map the field metallicity distribution in the LMC, and they present values of [Fe/H] (derived from Ca II IR triplet measurements) for 38 field red giants. Their distribution for [Fe/H] is shown in the top panel of Figure 7. This metallicity distribution peaks at about [Fe/H] $= -0.5$, with a fairly sharp cutoff at -0.25 and a diminishing tail down to [Fe/H] of about -1.6. Our sample of field stars is small, and the resulting [Fe/H] distribution is shown in the bottom panel of Figure 7; clearly, the overlap in metallicity between the two samples is perfect. The details of the shape of the metallicity distribution function for the field stars studied here cannot be well defined with only nine stars, so a detailed comparison with the Cole et al. (2000) results requires a larger sample, but the overall agreement is encouraging.

The two clusters sampled in this study have both had their metallicities measured by Olszewski et al. (1991), who also used the Ca II IR triplet method. For NGC 1898, they find [Fe/H] $= -1.37$, while we find [Fe/H] $= -1.13$ for member AM 5. With estimated total uncertainties of $\sim$0.16 dex in Fe I as derived from this study, plus the uncertainties from the Olszewski et al. work, a difference of 0.24 dex signifies

quite good agreement for this cluster. The other cluster common to both studies is NGC 2203, which has an average [Fe/H] = −0.64 from two members analyzed here (AM 1 and AM 2), while Olszewski et al. (1991) find [Fe/H] = −0.53, again quite good agreement between two very different types of analysis.

4.2. Sodium, Scandium, and Titanium Abundances

Commonly, results of stellar abundance analyses are expressed as the quantity [X/Fe]. The Na, Sc, and Ti abundances in Table 6 give mean values [Na/Fe] = −0.30, [Sc/Fe] = 0.0, and [Ti/Fe] = −0.18 with a star-to-star scatter most probably dominated by measurement errors. These results compare fairly favorably with measurements from LMC F–G supergiants and Cepheids: for example, Hill et al. (1995) give ([Na/Fe], [Sc/Fe], [Ti/Fe]) = (−0.2, −0.1, 0.0) for [Fe/H] ∼ −0.3 supergiants referenced to the Galactic supergiant Canopus, and Luck et al. (1998) give (−0.15, −0.14, 0.07) for similar Cepheids with respect to Galactic Cepheids. Use of Galactic comparisons minimizes systematic errors. At the same [Fe/H] as the LMC stars, Galactic stars show slightly positive values of [Na/Fe] and [Ti/Fe] but an [Sc/Fe] close to zero. The mild Na and Ti underabundances of the LMC stars relative to Galactic stars of the same [Fe/H] is likely attributable to the same factors responsible for the lower [O/Fe] (see below). In addition, the underabundances of Na and Ti, relative to Fe, are also found in the few dwarf spheroidal galaxies with published abundances (e.g., Shetrone, Côté, & Sargent 2001).

4.3. Carbon and Nitrogen Abundances

Carbon and nitrogen abundances are altered during mixing in red giants, as material exposed to the CN cycle is brought to the star's surface. The ^{12}C abundance decreases, the ^{14}N abundance increases, and the $^{12}C/^{13}C$ ratio decreases, but the sum of the ^{12}C, ^{13}C, and ^{14}N is conserved. This mixing in first-ascent and early AGB red giants is not expected to alter the ^{16}O abundance.

Figure 8 investigates the ^{12}C and ^{14}N abundances in the LMC red giants in comparison with other samples of stars, both in the LMC and in the Galaxy. The abundances of ^{14}N are plotted versus the abundances of ^{12}C. The solar symbol is located at $A(^{12}C) = 8.41$ (Allende Prieto, Lambert, & Asplund 2002, from their one-dimensional MARCS model) and $A(^{14}N) = 7.93$ (Holweger 2001). The solid curves are various "mixing curves" in which initial abundances of carbon and nitrogen are changed in such a way that their sum remains constant: as ^{12}C decreases, ^{14}N increases to mimic red giant mixing of material consisting of increasing exposure to the CN cycle. The open circles show the ^{12}C and ^{14}N abundances in Galactic disk M giants from Smith & Lambert (1985, 1986, 1990), and these giants are well represented by a CN-cycle mixing curve defined by approximately solar carbon and nitrogen initial abundances. The crosses are s-process–enriched MS and S stars, also from the Smith & Lambert papers, and are plotted with different symbols because the photospheres of these giants have presumably been contaminated by material from the third dredge-up, associated with ^4He-burning thermal pulses along the AGB. Such stars quite possibly have had primary ^{12}C added to their surfaces and might be expected to evolve away from a simple CN-cycle mixing curve. What should be noted con-
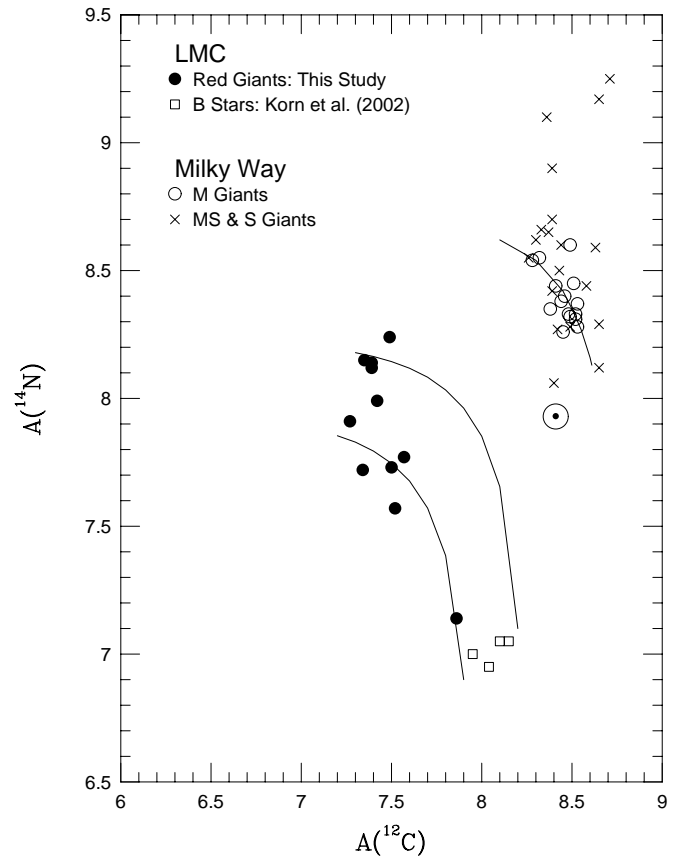

Fig. 8.—Abundances of ^{14}N vs. ^{12}C (on a scale with $A(X) = \log[n(X)/n(H)] + 12$) for the LMC red giants along with other LMC samples, as well as Galactic red giants (from Smith & Lambert 1985, 1986, 1990). The solid curves illustrate "CN mixing lines": since the CN cycle, operating by itself, will conserve the total C plus N nuclei, the curves represent these relations. No account is taken of some carbon cycled into ^{13}C; however, in the extreme case of the steady state CN cycle, this would shift the ^{12}C abundances by, at most, 0.1 dex toward lower values. In the case of the Galactic M giants, they are approximated reasonably well by CN-cycle mixing in nearly solar metallicity material. Some of the very ^{14}N-rich MS or S stars have converted some ^{16}O, or ^{12}C produced during ^4He burning, into nitrogen. The LMC red giants fall along CN mixing lines that are defined well by initial carbon and nitrogen abundances as derived by Korn et al. (2002) for main-sequence B stars in the young LMC cluster NGC 2004.

cerning the MS/S stars, however, are the few examples that show very large ^{14}N abundances. These objects are AGB stars that have undergone hot bottom burning (see, e.g., D'Antona & Mazzitelli 1996), where some amount of primary ^{12}C produced during thermal pulses on the AGB is converted to ^{14}N, via the CN cycle, at the base of a deep convective envelope.

The LMC red giants analyzed here are plotted in Figure 8 as filled circles and fall in a much different region than the Galactic red giants. The two mixing curves that define approximately the region in the carbon-nitrogen plane where the LMC giants fall begin at lower initial carbon and nitrogen abundances. As initial values, we used the recent paper by Korn et al. (2002) that presents abundances for four true main-sequence B star members of the young LMC cluster NGC 2004. They conducted a non-LTE abundance analysis, and their results for C and N are shown as squares in Figure 8. Using initial C and N abundances that bracket the Korn et al. (2002) abundances, the resulting CN-mixing curves provide excellent approximations to the behavior of

the field LMC red giants. One of the results for LMC initial abundances, as indicated by Korn et al. (2002), was a lower value for both [C/Fe] and [N/Fe] in the LMC: such mixing lines, beginning at values of about −0.3 dex in [C/Fe] and [N/Fe], go right through the regions defined by the red giant abundances. An additional conclusion from the comparison of the carbon and nitrogen abundances in both the main-sequence B stars and the red giants is that simple CN mixing does an excellent job of describing the dredge-up in this sample of red giants: no evidence of deeper mixing, or of hot bottom burning, is found. These processes might lower the star's ^{16}O abundance through conversion of some ^{16}O to ^{14}N through the ON cycles.

The constraint on possible oxygen depletions can be strengthened further by investigating the C/N abundance ratios. Most of the LMC giants in Figure 8 fall at values of [^{12}C/Fe] that are about 0.6–0.8 dex below their probable initial values (as suggested by the Korn et al. 2002 results). At these levels of ^{12}C depletions, for the case of only CN-cycle mixing, the expected C/N ratios would be about 6 or less; all of the measured C/N ratios calculated from the abundances in Table 6 fit this constraint. The C/N ratio will increase over this value if additional nitrogen is added from the conversion of ^{16}O to ^{14}N via the ON cycles. Because oxygen is the most abundant member of the CNO trio, even a relatively modest depletion will measurably increase the nitrogen abundance. Given a plausible initial oxygen abundance as determined by Korn et al. (2002), a decrease in ^{16}O of 0.2 dex would increase the C/N ratio to values of 8–10 in the regime of carbon depletions observed in the present sample of LMC red giants; such a large ratio is not found in any of the program stars. The LMC red giants studied here appear to have effectively unaltered ^{16}O.

The $^{12}C/^{13}C$ ratio is another abundance indicator that is sensitive to stellar mixing on the red giant branch. The initial ratio is expected to be quite large (~40–90), while first dredge-up lowers this ratio to ~18–26 for stars in the mass range from ~1 to 8 $M_{\odot}$ according to standard stellar models (e.g., Charbonnel 1994; but see Iben 1964). It has been known for some time that low-mass field giants exhibited lower $^{12}C/^{13}C$ ratios than predicted by standard models, with Keller, Pilachowski, & Sneden (2002) providing recent results of a discussion of this effect. Masses for giant star members of clusters can be determined more accurately than masses for field giants, and the effect of lower $^{12}C/^{13}C$ ratios in lower mass giants has been quantified by Gilroy (1989) using open clusters. Her results of $^{12}C/^{13}C$ versus giant mass are plotted in Figure 9 (squares). Above a mass of about 2.0–2.5 $M_{\odot}$, the values of $^{12}C/^{13}C$ are 22–30 and agree reasonably well with standard stellar models of first dredge-up. In the lower mass giants, however, Gilroy (1989) finds steadily decreasing $^{12}C/^{13}C$ ratios with decreasing mass, in contradiction to standard models. The $^{12}C/^{13}C$ ratios derived here for the LMC red giants are also plotted in Figure 9 (circles). The masses for the LMC giants are estimated to only ±0.5 $M_{\odot}$ and are based on the model tracks from Figure 2; these masses should be viewed as crude estimates. Nevertheless, there is a general trend of lower $^{12}C/^{13}C$ ratios with lower masses that tracks the Gilroy (1989) trend rather well, although offset to lower isotopic $^{12}C/^{13}C$ ratios for a given mass. Charbonnel (1994) and Charbonnel, Brown, & Wallerstein (1998) investigated the lower $^{12}C/^{13}C$ values in the lower mass red giants and suggest that extra mixing, possibly driven by meridional circu-
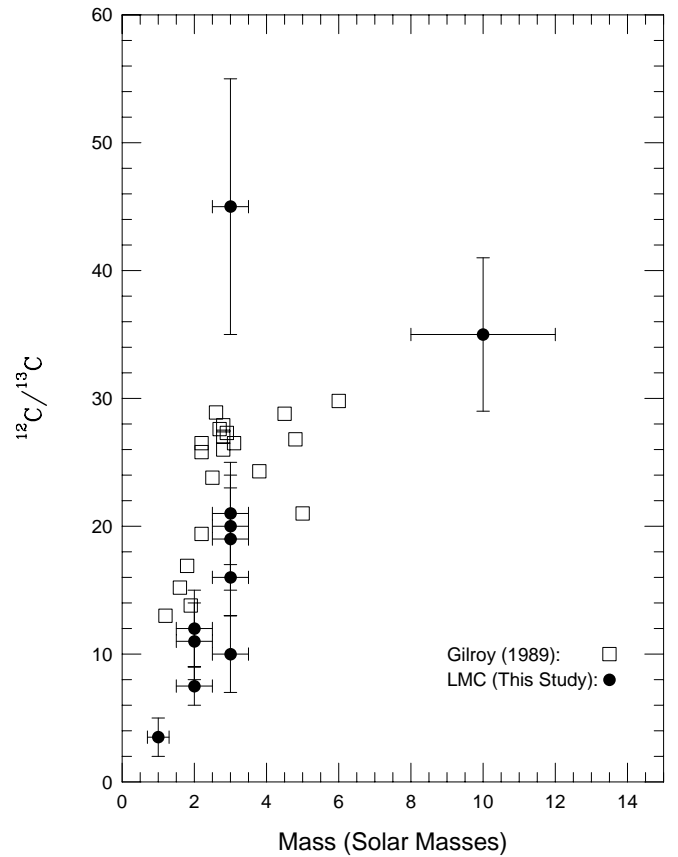

FIG. 9.—$^{12}C/^{13}C$ ratios vs. stellar mass in the LMC red giants and in Galactic open cluster giants from Gilroy (1989). The LMC masses are estimated from the evolutionary tracks of Schaerer et al. (1993). The trend of a lower $^{12}C/^{13}C$ ratio with a lower stellar mass observed in the LMC sample of giants is in qualitative agreement with the result found by Gilroy for the Galactic giants. The noticeable offset between LMC and Galactic trends may be due to an increase in extra-mixing efficiency on the giant branch with decreasing metallicity, as argued by Charbonnel et al. (1998).

lation and rotationally induced turbulence, can explain the lower $^{12}C/^{13}C$ ratios. In their model, extra mixing is inhibited by mean molecular weight gradients, which increase with increasing metallicity, so they predict more extensive mixing (and lower $^{12}C/^{13}C$ ratios for a given-mass giant) at lower metallicities. The offset between Gilroy's (1989) trend and the LMC trend may be due to this metallicity effect.

The $^{12}C/^{13}C$ ratio of 45 in NGC 2203 AM 2 deserves some mention. Although the error bars on this measurement are large, it still falls well above the trend of $^{12}C/^{13}C$ with mass found for the other LMC red giants. One possibility is that this star has begun dredge-up as an AGB star and some ^{12}C (produced from ^{4}He burning) has been added to the photosphere. If the ^{12}C abundance were increased by 0.15 dex as a result of such dredge-up, the observed current $^{12}C/^{13}C$ ratio of 45 would have been 30 before the addition of extra ^{12}C, within the scatter of the other red giants. Until more LMC red giants are observed, such an explanation of the anomalous position of NGC 2203 AM 2 in Figure 9 is speculation.

4.4. Oxygen Abundances

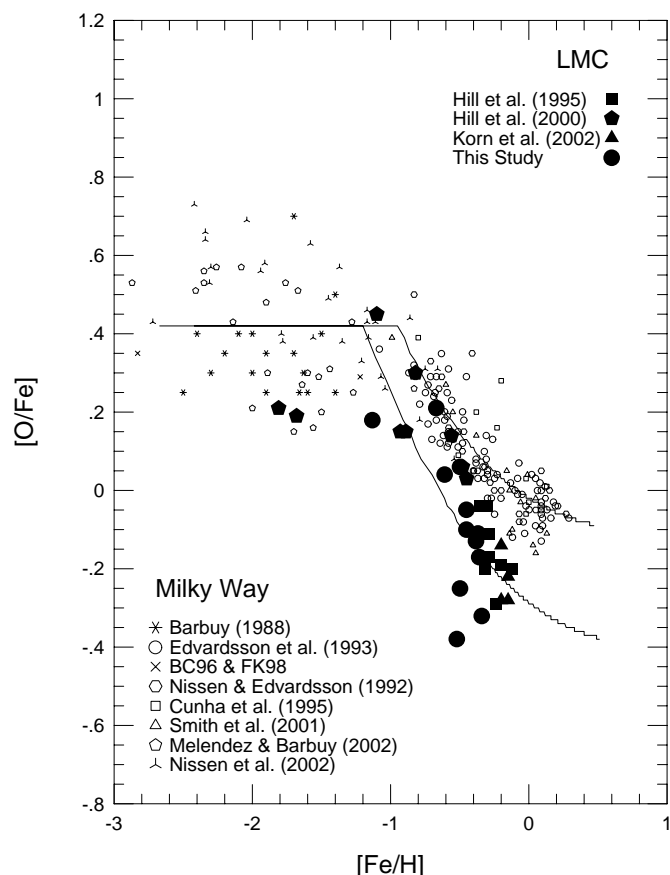On the assumption that the oxygen abundance is left unaltered by the convective mixing, an assumption sup-

FIG. 10.—Values of [O/Fe] vs. [Fe/H] for the LMC red giants, along with other samples of LMC and Galactic stars. Most of the Galactic results rely on the [O I] line near 6300 Å, weak O I lines near 6158 Å, or IR vibration-rotation OH lines (as used here). The LMC F supergiants from Hill et al. (1995) rely on the weak O I lines near 6158 Å, while the Korn et al. (2002) results for the hot B stars use lines of O II and Fe III. All three samples of LMC stars indicate a trend of [O/Fe] that falls ~0.2 dex below the Galactic trend at [Fe/H] ~ −0.5 to 0.0. The fact that three quite different samples of stars provide such a consistent result is a strong indication that [O/Fe] is low in the LMC compared with the Milky Way at near-solar values of [Fe/H]. The solid curves are simple models of chemical evolution in which supernovae of Type II and Ia add O and Fe into mixed gas. The LMC curve differs from the Milky Way curve by having an SN II rate that is 3 times lower and an SN Ia rate that is 2 times lower.

ported by the ^{12}C, ^{13}C, and ^{14}N abundances of the LMC red giants, the O/Fe ratio may be used as a tracer of chemical evolution. The [O/Fe] values run from −0.3 to +0.3 with a hint that they increase with decreasing [Fe/H]. Oxygen-to-iron abundances from a large number of Galactic and LMC studies, presented as [O/Fe] versus [Fe/H], are brought together in Figure 10: the LMC red giant results from this study are plotted as filled circles. The Galactic samples of field stars shown in this figure are taken from Edvardsson et al. (1993, *open circles*), Nissen & Edvardsson (1992, *hexagons*), Cunha, Smith, & Lambert (1995, *open squares*), and Smith, Cunha, & King (2001, *open triangles*) (the Galactic results are plotted as smaller symbols simply to keep these numerous points from falling on top of each other and obliterating their visibility). The open pentagons at low metallicity are the recent results for Galactic stars from Meléndez & Barbuy (2002) using the IR OH vibration-rotation lines; this paper also includes the earlier results from Meléndez et al. (2001). Other low-metallicity results for [O/Fe] are from

Barbuy (1988) and Nissen et al. (2002), shown as six- and three-pointed stars, respectively. Additional [O/Fe] values for the LMC are shown as comparisons with the red giants observed here: the filled triangles are from Korn et al. (2002) for main-sequence B stars, the filled squares are from Hill et al. (1995) for F supergiants, and the filled pentagons are from Hill et al. (2000) and Spite et al. (2001) for old clusters and globular clusters. Figure 10 shows that, over the metallicity range of [Fe/H] ~ −1.0 to −0.2, the LMC stars fall about 0.2–0.3 dex below stars in the Milky Way. The fact that main-sequence B stars, F supergiants, and cool red giants all yield the same results from independent analyses using very different sets of lines (O II and Fe III for B stars, weak O I 6158 Å lines and Fe II for F supergiants, and Fe I plus OH for the red giants) suggests strongly that this is now a well-established trend.

The common interpretation of the different [O/Fe]-[Fe/H] relations is that star formation in the LMC occurred in an early burst. Interruption of star formation reduced the input of oxygen into the interstellar gas. In this interval, SNe Ia delivered iron and so brought the O/Fe down. In the Galaxy, star formation was less affected by bursts, and O/Fe remained at its "high" value to a higher [Fe/H] than in the LMC. The solid curves shown in Figure 10 are a simple interpretation of the differing values of [O/Fe] in the Milky Way versus the LMC. These curves were generated by taking yields from supernovae of Types II and Ia and adding the processed elements into a unit mass of gas over time. The rate at which the abundances grow with time depends on the supernova rate per unit mass of gas. This rate is normalized by assuming a rate of one SN II per 100 yr and one SN Ia per 300 yr in the Milky Way, with the mass taken to be 10^{11} $M_{\odot}$. Oxygen mass yields for SNe II were taken from Arnett (1996) and convolved with a Salpeter mass function to yield an average mass of 1.5 $M_{\odot}$ ejected per SN II. Iron yields for SNe II were similar to that from Timmes, Woosley, & Weaver (1995) and set at 0.15 $M_{\odot}$ per SN II. With the rates and yields set for the Milky Way SNe II, it remained to set both the Fe yield from SNe Ia and the time delay for their initial contribution to chemical evolution. In order to fit the Milky Way trend as shown in Figure 10, it was necessary to set the SN Ia Fe yield to 0.7 $M_{\odot}$ per SN Ia and to use a time delay of 1.5 Gyr: both these values are reasonable in such a simple approximation. The resulting curve does a fairly good job of following the values of [O/Fe] versus [Fe/H] in the Milky Way, with the final point on the calculated curve shown being reached after a time of 12 Gyr. The other curve shown was generated as an approximation to the LMC trend of [O/Fe] versus [Fe/H]. Although not a unique solution, this curve was generated by simply lowering the SN II rate per unit mass in the LMC by a factor of 3 and the SN Ia rate by a factor of 2 (the SN II and SN Ia O and Fe yields and SN Ia time delay were the same). This very simple numerical model indicates that the [O/Fe] abundance ratios in the LMC can be understood as arising from both a slower rate of SNe II per unit mass (caused presumably by a lower average star formation rate per unit mass of gas) and a slightly enhanced ratio of SN Ia rates to SN II rates in the LMC. These results are in rough agreement with those suggested by the analytical chemical evolution models of Pagel & Tautvaišienė (1998).

5. CONCLUSIONS

Abundances of seven elements (C, N, O, Na, Sc, Ti, and Fe) have been measured in 12 red giant members of the LMC from high-resolution IR spectra obtained with Gemini South plus Phoenix. Using IR spectra, it is possible to extract quantitative chemical abundances for a number of elements in somewhat lower mass stars ($M \sim 2$–$4\ M_\odot$ red giants) in the LMC than previous high-resolution optical spectroscopic studies of main-sequence B stars or F to K supergiants (with $M \sim 8$–$10\ M_\odot$). The IR abundance analyses add complementary stellar-mass targets to the earlier works. In addition, the molecular lines of such species as CO, OH, or CN in the IR spectra allow for the determination of the abundances of specific CNO isotopic species, such as ^{12}C, ^{13}C, ^{14}N, and ^{16}O here, or ^{17}O, ^{18}O, and ^{15}N in future studies.

The iron abundances sampled here range from [Fe/H] $= -1.1$ to [Fe/H] $= -0.3$. Both [Na/Fe] and [Ti/Fe] are found to be consistently lower than their Galactic values by roughly -0.1 to -0.5 over the metallicity range sampled in the LMC. These characteristic underabundances of Na and Ti seem to also occur in a number of dwarf spheroidal galaxies (Shetrone et al. 2001).

The LMC red giants in this sample all show evidence of the mixing of CN-cycle material to their surfaces via the first dredge-up, with ^{14}N enhanced by $+0.4$ to $+0.8$ dex over its estimated initial values, and ^{12}C decreased by -0.3 to -0.5 dex. No evidence is found, in these predominantly first-ascent giants or early AGB stars, of the extreme nitrogen enrichments (about $+1.0$ dex or more) that might result from second dredge-up or hot bottom burning. The ^{12}C/^{13}C ratios in the LMC red giants are found to decrease with decreasing giant star mass in a manner similar to that found for Galactic red giants (Gilroy 1989); however, the LMC trend appears to be shifted to lower ^{12}C/^{13}C ratios for a given red giant mass. This shift may be due to the increased mixing associated with lower metallicity giants, as suggested by Charbonnel et al. (1998).

A comparison of [O/Fe] versus [Fe/H] between the LMC and the Milky Way finds that the LMC trend falls below by about 0.2 dex over the range of [Fe/H] $= -1.1$ to [Fe/H] $= -0.3$. Good agreement in [O/Fe] as derived from a sample of F supergiants (Hill et al. 1995), main-sequence B stars (Korn et al. 2002), and the red giants analyzed here suggests that the difference between the LMC and the Milky Way is real. Lower values of [O/Fe] in the LMC can be explained by both a lower supernova rate (caused by a lower star formation rate) and a lower ratio of Type II to Type Ia supernovae.

REFERENCES

Aaronson, M., & Mould, J. 1985, ApJ, 288, 551
Allende Prieto, C., Lambert, D. L., & Asplund, M. 2002, ApJ, 573, L137
Arnett, D. 1996, Supernovae and Nucleosynthesis (Princeton: Princeton Univ. Press)
Asplund, M., & García Pérez, A. E. 2001, A&A, 372, 601
Asplund, M., Gustafsson, B., Kiselman, D., & Eriksson, K. 1997, A&A, 318, 521 (erratum 323, 286)
Balachandran, S. C., & Carney, B. W. 1996, AJ, 111, 946
Barbuy, B. 1988, A&A, 191, 121
Barbuy, B., de Freitas Pacheco, J. A., & Castro, S. 1994, A&A, 283, 32
Bessell, M. S., & Brett, J. M. 1988, PASP, 100, 1134
Bessell, M. S., Castelli, F., & Plez, B. 1998, A&A, 333, 231 (erratum 337, 321)
Bica, E., Geisler, D., Dottori, H., Clariá, J. J., Piatti, A. E., & Santos, J. F. C., Jr. 1998, AJ, 116, 723
Carpenter, J. M. 2001, AJ, 121, 2851
Charbonnel, C. 1994, A&A, 282, 811
Charbonnel, C., Brown, J. A., & Wallerstein, G. 1998, A&A, 332, 204
Cole, A. A., Smecker-Hane, T. A., & Gallagher, J. S., III. 2000, AJ, 120, 1808
Costes, M., Naulin, C., & Dorthe, G. 1990, A&A, 232, 270
Cunha, K., Smith, V. V., & Lambert, D. L. 1995, ApJ, 452, 634
D'Antona, F., & Mazzitelli, I. 1996, ApJ, 470, 1093
Dopita, M. A., et al. 1996, ApJ, 460, 320
Edvardsson, B., Andersen, J., Gustafsson, B., Lambert, D. L., Nissen, P. E., & Tomkin, J. 1993, A&A, 275, 101
Geisler, D., Bica, E., Dottori, H., Clariá, J. J., Piatti, A. E., & Santos, J. F. C., Jr. 1997, AJ, 114, 1920
Gilroy, K. K. 1989, ApJ, 347, 835
Goldman, A., Shoenfeld, W. G., Goorvitch, D., Chackerian, C., Jr., Dothe, H., Mélen, F., Abrams, M. C., & Selby, J. E. A. 1998, J. Quant. Spectrosc. Radiat. Transfer, 59, 453
Goorvitch, D. 1994, ApJS, 95, 535
Gustafsson, B., Bell, R. A., Eriksson, K., & Nordlund, Å. 1975, A&A, 42, 407
Hill, V., Andrievsky, S., & Spite, M. 1995, A&A, 293, 347
Hill, V., François, P., Spite, M., Primas, F., & Spite, F. 2000, A&A, 364, L19
Hill, V., et al. 2002, A&A, 387, 560
Hinkle, K., Wallace, L., & Livingston, W. C. 1995, Infrared Atlas of the Arcturus Spectrum: 0.9–5.3 Microns (San Francisco ASP)
Hinkle, K. H., et al. 2002, Proc. SPIE, 4834, in press
Hinkle, K. H., Cuberly, R. W., Gaughan, N. A., Heynssens, J. B., Joyce, R. R., Ridgway, S. T., Schmitt, P., & Simmons, J. E. 1998, Proc. SPIE, 3354, 810

Hinkle, K. H., Joyce, R. R., Sharp, N., & Valenti, J. A. 2000, Proc. SPIE, 4008, 720
Holweger, H. 2001, in AIP Conf. Proc. 598, Solar and Galactic Composition, ed. R. F. Wimmer-Schweingruber (New York: AIP), 23
Huber, K.-P., & Herzberg, G. 1979, Constants of Diatomic Molecules (New York: Van Nostrand)
Iben, I., Jr. 1964, ApJ, 140, 1631
Keller, L. D., Pilachowski, C. A., & Sneden, C. 2001, AJ, 122, 2554
Korn, A. J., Becker, S. R., Gummersbach, C. A., & Wolf, B. 2000, A&A, 353, 655
Korn, A. J., Keller, S. C., Kaufer, A., Langer, N., Przybilla, N., Stahl, O., & Wolf, B. 2002, A&A, 385, 143
Kurucz, R. L., & Bell, B. 1995, CD-ROM 23, Atomic Line Data (Cambridge: Smithsonian Astrophys. Obs.)
Luck, R. E., Moffett, T. J., Barnes, T. G., III, & Gieren, W. P. 1998, AJ, 115, 605
McWilliam, A. 1990, ApJS, 74, 1075
Meléndez, J., & Barbuy, B. 2002, ApJ, 575, 474
Meléndez, J., Barbuy, B., & Spite, F. 2001, ApJ, 556, 858
Nissen, P. E., & Edvardsson, B. 1992, A&A, 261, 255
Nissen, P. E., Primas, F., Asplund, M., & Lambert, D. L. 2002, A&A, 390, 235
Olszewski, E. W., Schommer, R. A., Suntzeff, N. B., & Harris, H. C. 1991, AJ, 101, 515
Pagel, B. E. J., & Tautvaišienė, G. 1995, MNRAS, 276, 505
Plez, B., Brett, J. M., & Nordlund, A. 1992, A&A, 256, 551
Prévot, L., et al. 1985, A&AS, 62, 23
Russell, S. C., & Dopita, M. A. 1992, ApJ, 384, 508
Schaerer, D., Charbonnel, C., Meynet, G., Maeder, M., & Schaller, G. 1993, A&AS, 102, 339
Shetrone, M. D., Côté, P., & Sargent, W. L. W. 2001, ApJ, 548, 592
Smith, V. V., Cunha, K., & King, J. R. 2001, AJ, 122, 370
Smith, V. V., & Lambert, D. L. 1985, ApJ, 294, 326
———. 1986, ApJ, 311, 843
———. 1990, ApJS, 72, 387
Smith, V. V., Suntzeff, N. B., Cunha, K., Gallino, R., Busso, M., Lambert, D. L., & Straniero, O. 2000, AJ, 119, 1239
Sneden, C. 1973, ApJ, 184, 839
Spite, M., Hill, V., Primas, F., François, P., & Spite, F. 2001, NewA Rev., 45, 557
Timmes, F. X., Woosley, S. E., & Weaver, T. A. 1995, ApJS, 98, 617